

# Distributed-Flap Layout Trade Study on a Highly Flexible Common Research Model

David L. Rodriguez\*

*Science & Technology Corp., Moffett Field, CA 94035*

Michael J. Aftosmis† and Marian Nemec‡

*NASA Ames Research Center, Moffett Field, CA 94035*

George R. Anderson§

*Science & Technology Corp., Moffett Field, CA 94035*

The results of a layout trade study of a full-span, trailing-edge flap system for the NASA Common Research Model are presented. Previously developed analysis and design tools are used to determine the potential performance benefits of several flap layouts on a highly flexible version of the aircraft wing. The wing is first re-twisted for optimal aerodynamic performance at the design cruise condition while addressing aeroelastic effects. Several flap layouts are then installed on the new baseline wing. The deflection of each segment on all flap layouts is then optimized for aerodynamic performance at an overspeed flight condition to ascertain the effectiveness of each flap system. The results indicate that employing two-segment flaps greatly improves overspeed performance as compared to using no or just single-segment flaps. The study also showed that additional segments offer only incremental improvements in performance. The results also show that using only four spanwise flaps can produce meaningful performance gains. Overall, the trade study results suggest a simple distributed flap system (four spanwise flaps with two segments each) can reduce the drag of the Common Research Model by 13 counts at a Mach number that is 3.5% higher than the design cruise point.

## Nomenclature

$C_D$	=	drag coefficient
$C_L$	=	lift coefficient
$C_{L,cruise}$	=	design cruise lift coefficient
$C_{L,max}$	=	maximum lift coefficient
$C_M$	=	pitching moment coefficient
$C_p$	=	pressure coefficient
$i_t$	=	horizontal tail incidence
$x/c$	=	chordwise fraction
$M_\infty$	=	freestream Mach number
$\alpha$	=	flight angle of attack
$\alpha_{max}$	=	maximum allowed flight angle of attack at cruise
$\Delta$	=	distributed flap deflections
$\theta_w$	=	spanwise wing twist distribution

## I. Introduction

The weight of a transport aircraft will vary significantly throughout a typical long-range flight mission due to fuel-burn. Transport wings are usually designed for either a single cruise flight condition or by using a weighted

---

\* Senior Research Scientist, Computational Aerosciences Branch, MS 258-5; [david.l.rodriguez@nasa.gov](mailto:david.l.rodriguez@nasa.gov), Senior Member AIAA.

† Aerospace Engineer, Computational Aerosciences Branch, MS 258-5; [michael.aftosmis@nasa.gov](mailto:michael.aftosmis@nasa.gov), Associate Fellow AIAA.

‡ Aerospace Engineer, Computational Aerosciences Branch, MS 258-5; [marian.nemec@nasa.gov](mailto:marian.nemec@nasa.gov), Senior Member AIAA.

§ Research Scientist, Computational Aerosciences Branch, MS 258-5; [george.anderson@nasa.gov](mailto:george.anderson@nasa.gov), AIAA Member.

combination of multiple design flight conditions. Such a compromise is made to produce a wing that has near-optimal performance for most of the cruise segment of the mission, but this means that the wing design is rarely optimal for any particular flight condition. Step-climb trajectories can reduce this deviation from the optimum, and continuous cruise-climb can effectively eliminate it. However, increasing air traffic has limited the utility of these trajectories, especially in the case of cruise-climb. To compound matters, modern aircraft wings are becoming increasingly flexible due to the use of composite materials to reduce weight. For instance, the Boeing 787 Dreamliner exhibits roughly a 10% semispan wing-tip deformation at cruise, which is nominally twice what similar aircraft with aluminum wings exhibit. As the aircraft weight decreases throughout cruise, the shape of such a flexible wing dramatically varies, making it more challenging to maintain optimum performance at any given flight condition.

Modern airplanes such as the Boeing 787 and Airbus A350 employ cruise flaps to improve performance. Exploiting the same principles, a related concept is the Variable-Camber Continuous-Trailing-Edge Flap (VCCTEF) system proposed by Nguyen<sup>1</sup> and further studied by Nguyen et al.,<sup>2</sup> Urnes et al.,<sup>3</sup> and Rodriguez et al.<sup>4</sup> This concept consists of an array of multi-segmented, rigid flaps that are distributed along most of the span of the wing. It is a subset of the variable camber concept described by Spillman<sup>5</sup> and is similar to that presented by Szodrach and Hilbig.<sup>6</sup> While these earlier concepts used trailing edge flaps segmented in the chordwise direction, the VCCTEF design also seals the gaps between span-adjacent flaps with an elastomer material to reduce local losses and noise. The segmented flaps of the VCCTEF system also make it distinct from morphing trailing edge concepts such as the Adaptive Compliant Trailing Edge<sup>7</sup> and FlexSys system,<sup>8</sup> where the entire flap and internal structure maintain a smooth shape in both the chordwise and spanwise directions. Note that concurrent to the overall VCCTEF study, Burdette et al.<sup>9</sup> have studied similar morphing trailing edge geometries on the NASA Common Research Model<sup>10</sup> by conducting high-fidelity, aeroelastic analysis over an entire typical mission.

In a previous work,<sup>4</sup> a VCCTEF system on the NASA Generic Transport Model (GTM)<sup>11</sup> was evaluated at several off-design cruise conditions. The GTM wing was analyzed assuming a modern composite structure which resulted in greater wing deformation than the nominal design. This “softened” GTM wing was redesigned using previous developed tools<sup>4,12</sup> at the mid-cruise point of a notional mission profile. The deflections of the VCCTEF system were then optimized at three off-design conditions to evaluate the flap system’s effectiveness in improving performance. Of these off-design conditions, the overspeed condition (3.8% greater than the design cruise Mach number) in particular showed significant decrease in performance that could be mostly offset by re-optimizing the flap system deflections. These initial results suggest that a distributed flap concept could be quite effective at mitigating increased transonic wave drag in overspeed flight conditions and motivate the present work. Since the flap layout was fixed in the previous work, it is not clear how elaborate a distributed flap system must be to effectively improve performance at an overspeed condition. Naturally, simpler flap systems are preferable for reduced complexity and weight considerations. This uncertainty is investigated in the present work via a more thorough flap layout trade study. Several flap system layouts with varying number of spanwise and chordwise segments are analyzed and optimized at a typical overspeed condition. A sufficiently comprehensive flap layout trade study should provide guidance to a designer on the tradeoff between added mechanical complexity and robust aerodynamic performance.

## II. Methodology

The aerodynamic analysis and design tools used to complete the trade study of the distributed flap system are identical to those used in past work.<sup>4</sup> In this section, the static aeroelastic analysis method<sup>12</sup> previously developed by the authors is summarized. This method was then incorporated within a proven optimization framework<sup>13</sup> to allow for aerodynamic design that includes aeroelastic effects. This design optimization method was used to conduct the trade study of the distributed flap system on the NASA Common Research Model (CRM).<sup>10</sup> The methods used to geometrically model the distributed flap system are also summarized.

### A. Static Aeroelastic Analysis

A classic, loosely-coupled, iterative technique was used to conduct static aeroelastic analysis of transport wings (Figure 1). The process begins by aerodynamically analyzing the baseline geometry and building a structural model which fits within the outer mold line of the wing. The aerodynamic analysis is performed by an automated, inviscid, cut-cell Cartesian method (Cart3D<sup>14</sup>). The wing aerodynamic load distribution is then transferred to the structural model. A shell-beam finite element solver (BEAM<sup>15</sup>) calculates the structural response to the provided load distribution. The computed deformation of the wing is applied to the baseline geometry and the process is repeated until the wing deformation shape converges, thus producing a consistent set of loads and deformations. The method has proven to be robust, efficient, and typically converges in about 5-6 iterations, even on very flexible wings. Reference 12 provides full details along with verification and validation of the method on flexible transport wings.

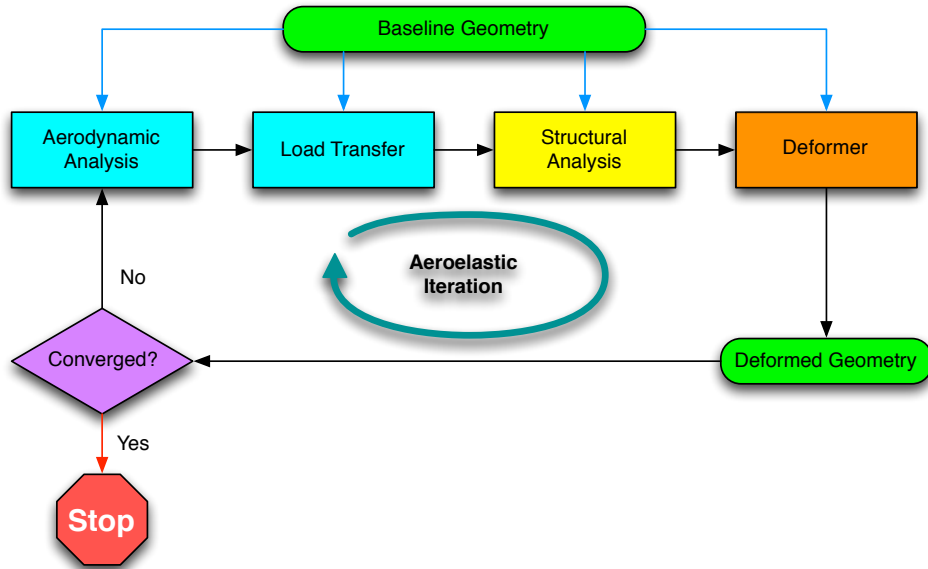


Figure 1. Architecture of the static aeroelastic analysis method.

### B. Aerodynamic Shape Optimization with Aeroelastic Effects

The Cart3D design framework<sup>13</sup> has been successfully used to perform aerodynamic shape optimization for many problems, some of which are presented by Aftosmis,<sup>16</sup> Wintzer,<sup>17</sup> and Smith.<sup>18</sup> The method uses a flow adjoint solver to compute objective and constraint function sensitivities to user-defined design variables, allowing for the use of efficient gradient-based optimization techniques. The framework has been shown to be very effective in optimizing complex geometries in inviscid flow.

While the method has mostly been applied to rigid geometries, the authors have extended the framework to accommodate static aeroelastic effects.<sup>4</sup> With some minor enhancements, the aeroelastic analysis algorithm described in Figure 1 has been used to perform aerodynamic shape optimization of flexible wings with a fixed structural layout. The loosely-coupled analysis method was wrapped within an iterative loop as shown in Figure 2. In applying this architecture, a baseline geometry is first analyzed with the aeroelastic analysis method (Figure 1) to compute the deformed shape of the wing. This change in the wing shape due to aeroelastic effects is then held constant throughout a subsequent aerodynamic shape optimization procedure. For any evaluation in the wing optimization, the shape design variables (local wing twist or flap deflections in this work) are first applied to the undeformed wing. The wing is then deformed according to the prediction of the aeroelastic analysis on the unoptimized wing. In other words, within each aeroelastic design iteration, the twist distribution and flap deflections of the wing are optimized while assuming the aeroelastic effects are constant.

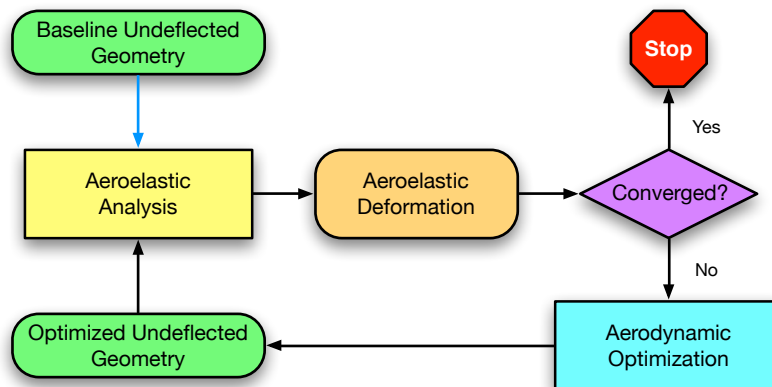


Figure 2. Architecture of the static aeroelastic design optimization method. The aeroelastic analysis block (yellow) is the process in Figure 1.

Of course, once the wing is optimized, the spanwise load distribution may be altered which modifies the deformed shape. The optimized wing is then analyzed again with the aeroelastic analysis tool, generating an updated deformed shape. This outer loop repeats until the deformed shape and the aircraft performance converges, thereby producing a wing design with near-optimal aerodynamic performance while modeling aeroelastic effects at the design flight condition. As will be shown later, this process has been observed to converge in just 3-4 outer loop iterations, resulting in a very efficient design tool for flexible wings. A tacit assumption of this approach is that the aeroelastic sensitivities are nearly linear. Nonlinearities in the effects of the aeroelastic deformation and thus induced drag, for instance, are assumed to be minimal. More details on this design technique are given in Reference 4.

### C. Modeling the Distributed Flap System

Geometric modeling of a large number of separate flap segments and the elastomer material between them presents an enormous challenge to traditional surface meshing techniques. A discrete surface model (required by the aerodynamic analysis) must be able to smoothly stretch and bend just as the elastomer material would in reality. Fortunately, 3-D soft-body animation tools are very accustomed to morphing geometric objects in a smooth and realistic fashion. The Blender\* discrete geometry modeler is an open-source tool, which has already been effectively used for shape optimization<sup>19</sup> and also with the aeroelastic analysis method.<sup>12</sup> For this work, the Blender modeler has been further enhanced to install a distributed flap system on a typical transport wing geometry. This augmented tool also enables interactive or scripted deflection of each chordwise segment of each flap.

Blender provides many ways of deforming discrete geometry objects. In this instance, a skeletal metaphor is employed to control the morphing of the surface mesh of a wing. By analogy, “bones” are armature elements bound to the “skin” and as these bones rotate and move, the bound surface triangles move with them. The degree of influence of each bone can be set for each surface mesh point. For instance, a flap segment could be bound so that each point within the flap boundary is completely under the influence of just one bone. But for the regions between flaps, the bones of the neighboring flaps have different levels of influence on each surface point. These regions are then able to mimic the physical behavior of the elastomer material. Figure 3 portrays an example deflection of flap bones, along with the corresponding morphed surface. This deflection is exaggerated to clearly demonstrate how the flap segments follow the bone rotations and the elastomer regions stretch to maintain a continuous trailing edge. More details of this geometric modeling of distributed flaps on a discrete surface are given in Reference 4.

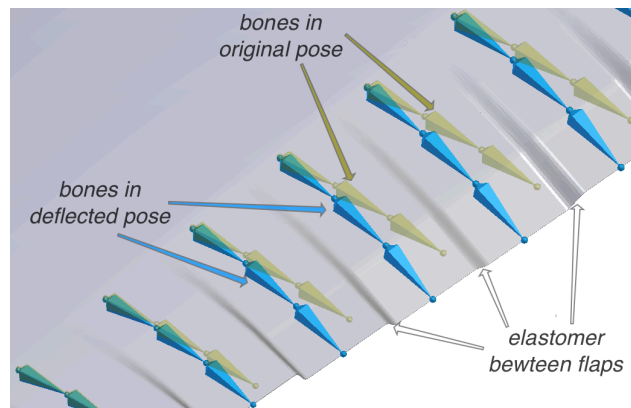


Figure 3. Sample deflection of flap bones. Gold translucent bones show the original orientation.

## III. Results

The methods presented in the previous section were applied to conduct a trade study on a distributed flap system layout. While the previous work was performed on the GTM,<sup>20</sup> the work presented here focuses on the more modern CRM.<sup>10</sup> Figure 4 illustrates this geometry that includes the fuselage, wing, and horizontal tail. The work consists of two steps. First the wing is re-twisted for near-optimal aerodynamic performance at nominal cruise conditions. Aeroelastic effects are addressed and the wing structure is designed to be about twice as flexible as the original CRM design. Second, several flap layouts are installed on the re-twisted CRM wing. The deflection of these flaps are then optimized at an overspeed, off-design flight condition. The results of the trade study are then discussed.

\* <https://www.blender.org>

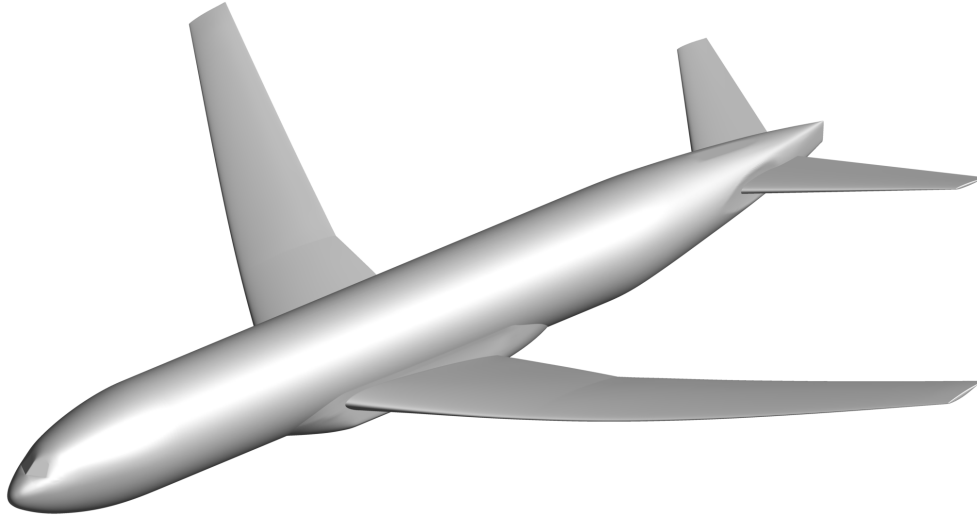


Figure 4. CRM geometry including fuselage, wing, and horizontal tail.

### A. Establishing a New Baseline

According to Vassberg et al,<sup>10</sup> the original CRM twist distribution was designed to perform well aerodynamically over a small range of flight conditions centered around the cruise point of Mach 0.85 with a lift coefficient of 0.5. Constraints on wing thickness and spanwise loading were enforced during the design, presumably to accommodate an internal structure though details were not presented in Reference 10. The original CRM geometry incorporates the aeroelastic deformation at the design point which assumes a conventional aluminum structure. However, this work assumes a much more flexible, composite wing structure that exhibits over twice as much wing tip deformation at the design point as the original design. The structural model used in this work was accordingly built to produce that magnitude of tip deformation. This shell-beam structural model was arbitrarily constructed with linearly tapering wing spar areas and web thicknesses and to fit within the outer mold line of the wing (for more details on the structural model, see Reference 15). The resulting bending and torsional stiffness distributions of the structural model are shown in Figure 5.

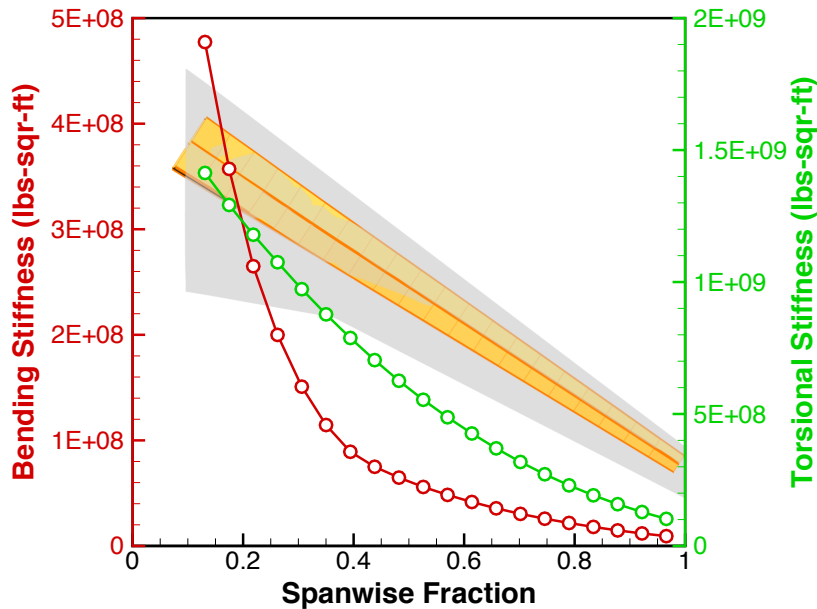


Figure 5. Bending and torsional stiffness distributions on highly flexible CRM wing.

In previous work on the GTM, the weights of the engine, fuel, and structure itself were all included in the aeroelastic analysis. Since the GTM was based on an actual aircraft design, the weights of these components were either known or could be estimated rather easily. The CRM, on the other hand, is not a fully realized aircraft design since its original purpose was to act as a validation platform for aerodynamic analysis methods.<sup>21</sup> Hence, the weights of these components are not known. Including these component weights is not crucial for this study since only the final deformed shape is desired. Alternatively, one could assume these additional component weights are actually built into the structural model used for this work.

To achieve near-optimal aerodynamic performance at cruise, the CRM wing jig-shape was re-twisted to create a new baseline design. Note the jig-shape was first created by straightening out the original CRM wing geometry which incorporated the cruise aeroelastic deformation. Aeroelastic effects were necessarily addressed in this re-design by employing the methods summarized in Section II. In addition, as was done by Chen et al<sup>22</sup> in their aerodynamic shape optimization of the CRM, a longitudinal trim constraint was also enforced by allowing the design method to alter the incidence of the horizontal tail. The center-of-gravity for this trim constraint was assumed to be at 25% mean aerodynamic chord, which is also the reference point specified by Vassberg<sup>10</sup> and used by Chen.<sup>22</sup> The optimization problem used to produce this new wing design can be summarized as follows:

$$\begin{aligned}
 &\text{minimize:} && C_D(\alpha, \boldsymbol{\theta}_w, i_t) \\
 &\text{subject to:} && C_L(\alpha, \boldsymbol{\theta}_w, i_t) = C_{L,cruise} = 0.5 \\
 &&& C_M(\alpha, \boldsymbol{\theta}_w, i_t) = 0 \\
 &&& \alpha \leq \alpha_{max}
 \end{aligned} \tag{1}$$

where  $\alpha$  is the flight angle of attack,  $\alpha_{max}$  is the maximum allowable angle of attack (to enforce a reasonable constraint on cabin deck angle),  $\boldsymbol{\theta}_w$  is the twist distribution over the span of the wing,  $i_t$  is the incidence of the horizontal tail,  $C_D$  is the aircraft drag coefficient,  $C_L$  is the lift coefficient, and  $C_M$  is the pitching moment coefficient about the reference point. In the end, this optimization is really just the classic problem of drag-minimization at fixed lift with the added longitudinal trim constraint. For this work,  $\alpha_{max}$  is arbitrarily set to  $3^\circ$ .

For the redesign of the more flexible CRM wing, the design variables in the optimization problem included the flight angle of attack to satisfy the lift constraint, the horizontal tail incidence to satisfy the pitching moment constraint, and the twist distribution of the wing. The twist distribution was varied discretely at the six spanwise stations shown in Figure 6. Between these stations, the change in the wing twist was varied linearly, thus producing a piecewise linear change in the spanwise twist distribution of the original CRM wing. Note the results from Reference 4 suggested that the incidence of the wing at the side of the fuselage had a strong effect on the aerodynamic performance of the generic transport. Consequently, the root incidence of the CRM wing was allowed to vary. Fortunately, the CRM fuselage geometry includes a landing gear pod that has a relatively flat surface at the wing intersection, which allows for some change in the wing root incidence with no loss in geometric integrity. The design framework is also capable of handling this change in the wing root incidence since it can easily re-intersect the wing with the fuselage.

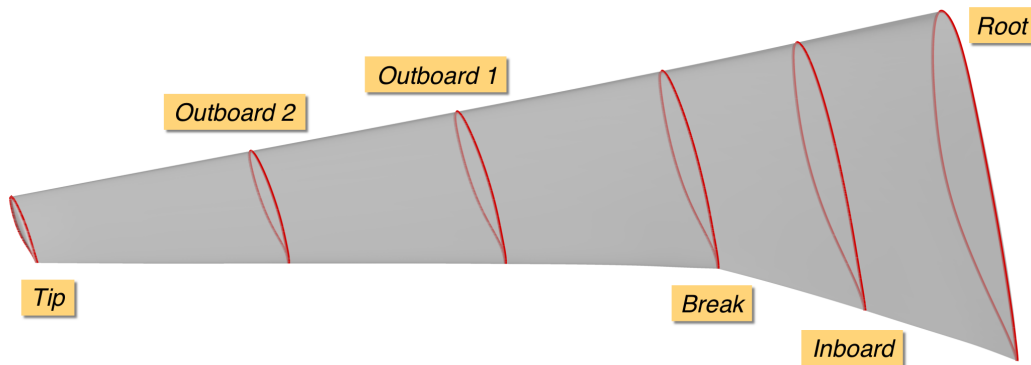


**Figure 6. Spanwise stations (red profile curves) used as twist design variables in CRM wing optimization.**

The aeroelastic design method shown in Figure 2 was applied to the problem stated in Eq. (1) to obtain an optimized, highly flexible CRM wing design. The convergence of this design optimization problem is shown in Fig-

ure 7. Recall that each point in the plot is a twist optimization with fixed wing deformation. The red curve shows the inviscid drag resulting from each design optimization. Note that the drag drops about 10 counts and converges rather quickly, reaching within 0.5% of its final value by the second design iteration. The blue curve shows the vertical wing tip deformation from the jig shape at each design iteration. The final wing tip deformation is about 147 inches, which is over 12% of the wing semispan. The tip deformation converged to within an inch of its final value in just two design iterations. The convergence of the actual design variables, including the horizontal tail incidence, is shown in Figure 8. This plot shows the design variables truly settle into their final values by the third design iteration. Though not shown in the plot, the final angle of attack was the constrained value of  $3^\circ$ .

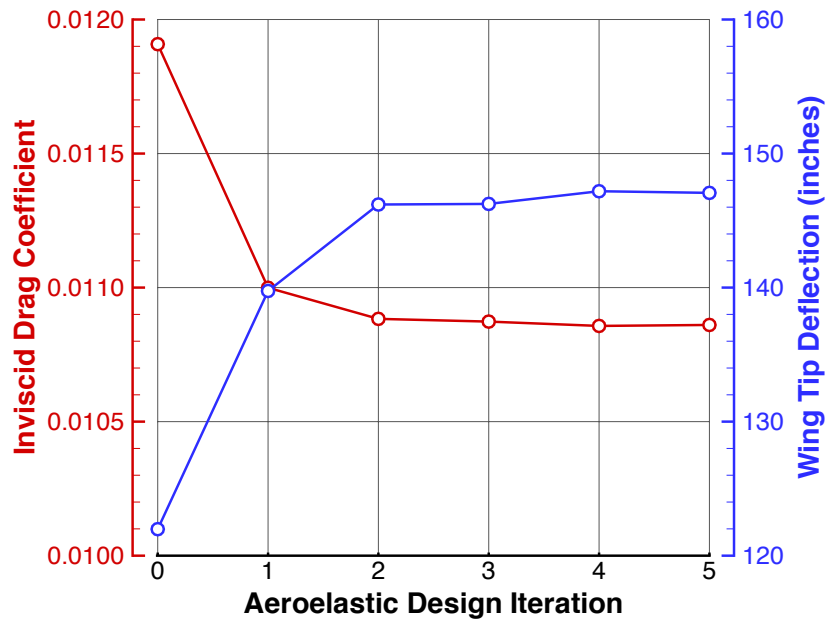


Figure 7. Convergence of highly flexible CRM design optimization at cruise.

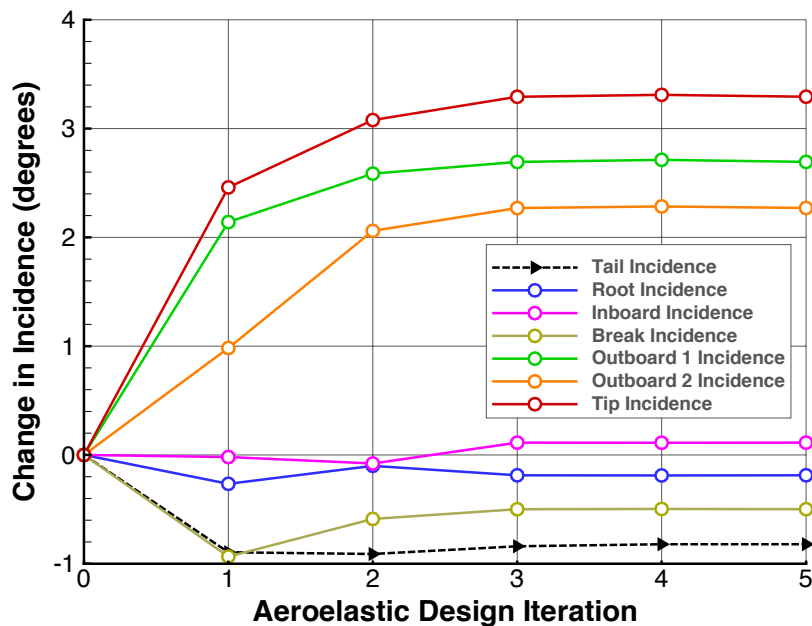


Figure 8. Convergence of twist variables in optimization of highly flexible CRM at cruise.

Computing accurate pitching moment values and gradients can be a challenge for high-fidelity aerodynamic analyses. The downwash of the wing must be computed accurately from the wing trailing edge to the horizontal tail since the tail has such a large effect on the pitching moment. Thus the pitching moment was the driving metric of the computational mesh size necessary for effective design optimization. Meshes of 30-50 million cells were necessary for each design iteration shown in Figure 7. For each aeroelastic design iteration, roughly 10-20 objective function evaluations were needed. Typically in the first few aeroelastic design iterations (cycles with fixed deformation), the design optimization process was not always fully converged to save computational resources. In fact, it was often not necessary to tightly converge a fixed-deformation optimization until that deformation approached convergence itself. With these large mesh sizes, a typical objective function and gradient evaluation required about 4-6 hours of wall clock time on a modern shared memory machine using 256 processing cores.

The final change in twist distribution determined by this aeroelastic optimization is shown in Figure 9. Small changes were needed near the root of the wing while significant increases in wing incidence were applied to the outboard wing sections. This was expected as the increased flexibility and therefore deformation of a backward swept wing decreases span loading near the tip. The aeroelastic optimization method reduced the CRM wing washout to recover this loss in outboard wing lift. The lift distribution on the original CRM configuration but with the more flexible structure is shown in Figure 10 along with that of the re-optimized wing. While the optimal wing loading for a trimmed wing-fuselage-tail configuration is not truly elliptical,<sup>23</sup> the lift distribution on the entire aircraft (black circles in Figure 10) is closer to an elliptic lift distribution than the original CRM configuration (black triangles in Figure 10) and is similar to the optimized trimmed lift distribution reported in Chen.<sup>22</sup> Note that Chen was not able to alter the wing-fuselage intersection in his work.

Recall that both the original and optimized CRM configurations were trimmed (zero pitching moment about the reference point), and that the optimized wing exhibits increased lift on the outboard portion of the wing which is behind the reference point. This increases the nose-down pitching moment induced by the wing that must be mitigated by an increased nose-up moment from the tail. This is verified by the increased down force on the horizontal tail shown in Figure 10. Figure 11 shows the pressure distributions on the original and optimized CRM configurations. This figure suggests that the reduction in cruise drag may not be exclusively due to induced drag reduction. The optimized wing exhibits less wave drag on the inboard part of the wing as indicated by the weaker shocks. On the other hand, the outboard wing shock is a bit stronger since it must carry more lift to compensate for the increased tip deformation.

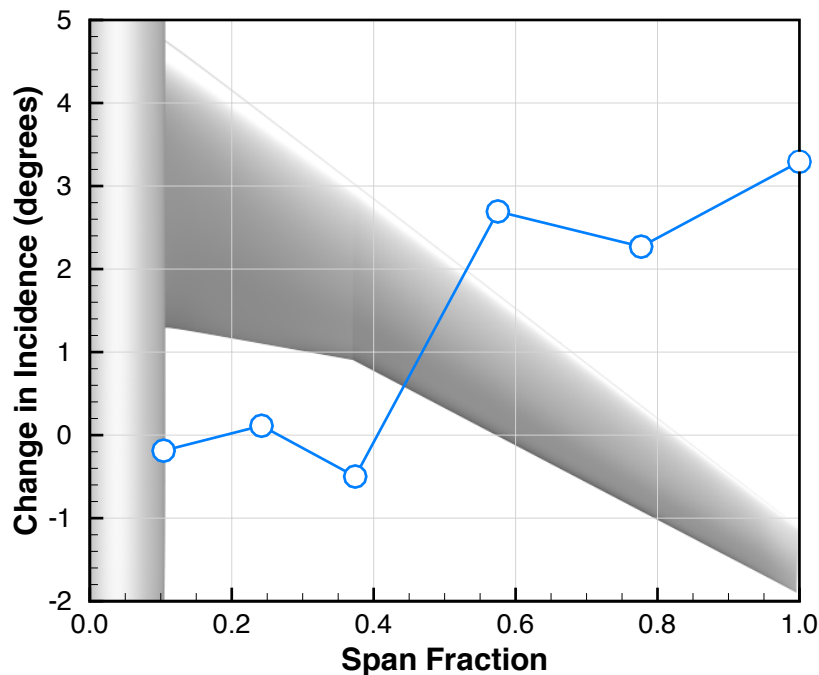


Figure 9. Change in twist distribution of highly flexible CRM wing optimized for cruise.

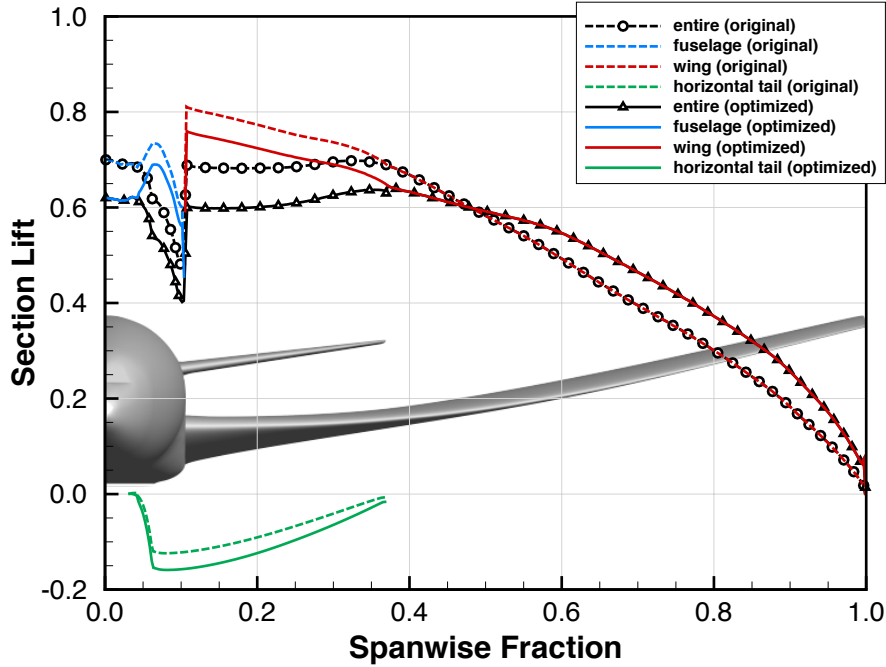


Figure 10. Lift distribution on original and optimized CRM configurations with highly flexible structure at cruise conditions ( $M_\infty = 0.85$ ,  $C_L = 0.5$ ).

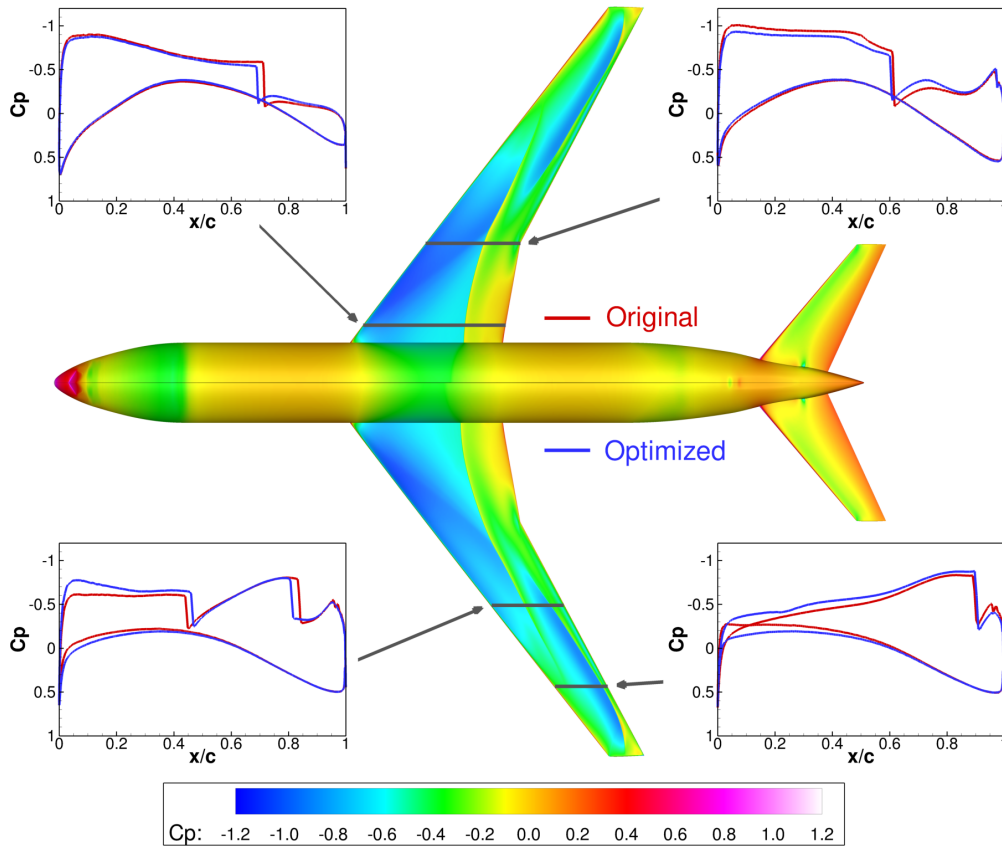


Figure 11. Pressure distributions on original and cruise-optimized CRM configuration with highly flexible wing structure ( $M_\infty = 0.85$ ,  $C_L = 0.5$ ).

## B. Flap Layout Trade Study

An overspeed flight condition was chosen for the CRM trade study since Reference 4 suggested it would provide a great opportunity for a distributed flap system to deliver a significant increase in aerodynamic performance. The overspeed condition selected assumed the aircraft had the same weight but was simply flying at a Mach number of 0.88 (3.5% increase over the design cruise point) at the same cruise altitude. This overspeed condition would, for example, reduce a 5 hour flight by roughly 10 minutes and perhaps overcome a gate arrival delay. Avoiding such a delay could prove less costly to an airline than the extra fuel burned by flying faster. Flying the optimized aircraft from Section A at increased speed at the same altitude lowers the cruise lift coefficient to  $C_L = 0.467$  but increases inviscid drag by over 15 counts (Figure 7).

Recall that the purpose of this flap layout trade study was to help determine how complex a distributed flap system would need to be in order to effectively improve the performance of the CRM flying at the higher Mach number. Starting with the newly re-optimized and highly flexible CRM wing presented in Section A, several distributed flap layouts were installed and optimized at the overspeed condition. These layouts had varying numbers of chordwise segments and spanwise flaps. For the most of the work in Reference 4, the chordwise deflection of each segment of a flap was strictly enforced to be “circular”, meaning that each flap deflected the same amount relative to its own hinge line. This deflection is illustrated in Figure 12. However, for the overspeed condition, this chordwise pattern of flap deflection was overly restrictive and not effective at improving performance. Conversely, allowing independent deflection of each chordwise segment during a design optimization did prove to be very effective in improving performance by reducing wave drag. Therefore, for the trade study presented here, each segment of each flap was allowed to deflect independently.

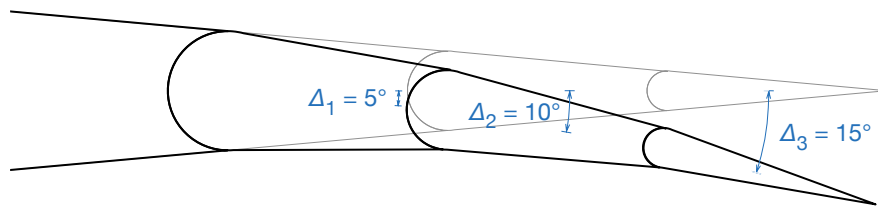


Figure 12. Example “circular” deflection of a flap with three chordwise segments.

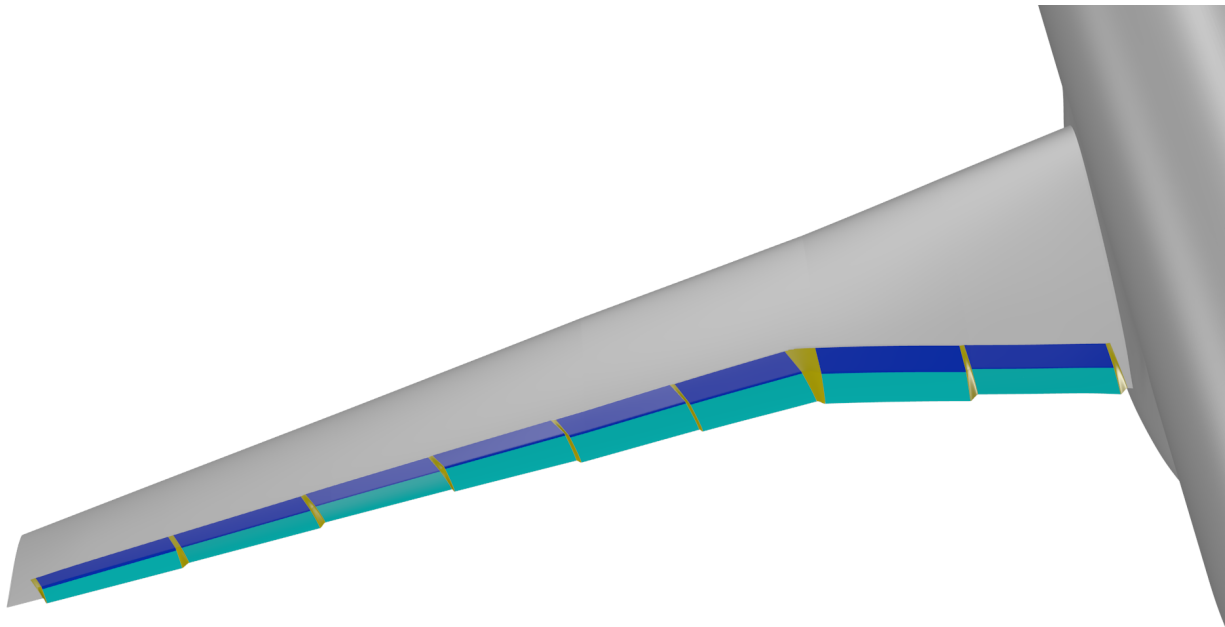


Figure 13. Example distributed flap installation on CRM wing. This system has 8 spanwise flaps, each with 2 chordwise segments (dark and light blue elements). The gold-colored material is the elastomer.

The GTM VCCTEF layout in Reference 4 had 16 spanwise flaps, each with 3 chordwise segments. The primary goal of the present work is to determine how complex a flap system is actually needed to get a worthwhile benefit at an overspeed condition. Hence, for this work, the number of spanwise flaps and the number of chordwise segments was varied. An elastomer material was installed in any gap between neighboring flaps and the end flaps and wing. A typical installation of the flap system is shown in Figure 13. The flap deflections in the illustration are somewhat random and exaggerated simply for clarity in the image.

The first set of flap systems considered used only 4 spanwise flaps with 1-3 chordwise segments each. These are depicted in Figure 14. The different shades of blue represent individual chordwise flap segments. Note the one-segment layout (4 x 1) is the simplest flap system considered in the entire trade study. Each layout in Figure 14 was optimized at the overspeed condition using the aeroelastic optimization procedure shown in Figure 2. The lift was constrained to the overspeed cruise value ( $C_L = 0.4665$ ) and the horizontal tail incidence was allowed to vary to maintain trim in pitch ( $C_M = 0$ ). This optimization problem is identical to that specified in Eq. (1). However, in contrast to the design problem in Section A, the twist distribution was held constant and the deflection of each segment of each flap was optimized.

The inviscid drag values as well as other performance metrics of these optimized configurations are shown in Table I along with the performance of the baseline wing with no flaps. The drag from each optimized system is also shown in Figure 15 as a bar chart for better visualization. First, note the significant decrease in drag (almost 4 counts) just by deflecting the 4 one-segment flaps (4 x 1). Secondly, note the two-segment flaps (4 x 2) improve performance even more significantly (another 9 counts, for a total of 13 from the baseline). The trend does not continue, however, as the three-segment flaps (4 x 3) do not provide significant performance benefit over the two-segment flaps (about half a count). This is the first notable finding from this trade study. The one-segment flaps are effective but not nearly as effective as the two-segment flaps. Adding a third segment is not appreciably advantageous, particularly when considering the added weight of another set of hinges and actuators. At this point, it makes sense to understand why two-segment flaps perform so well.

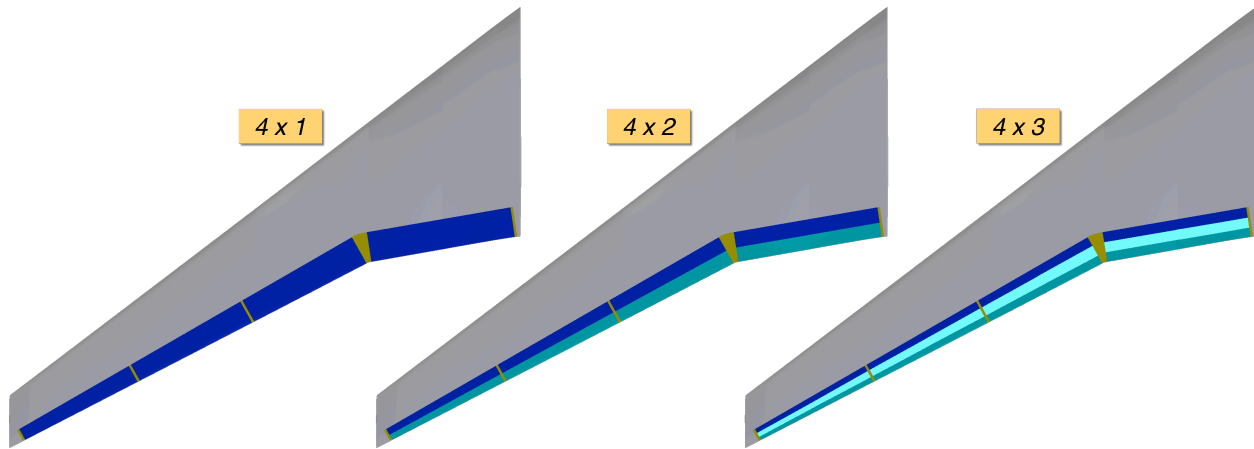
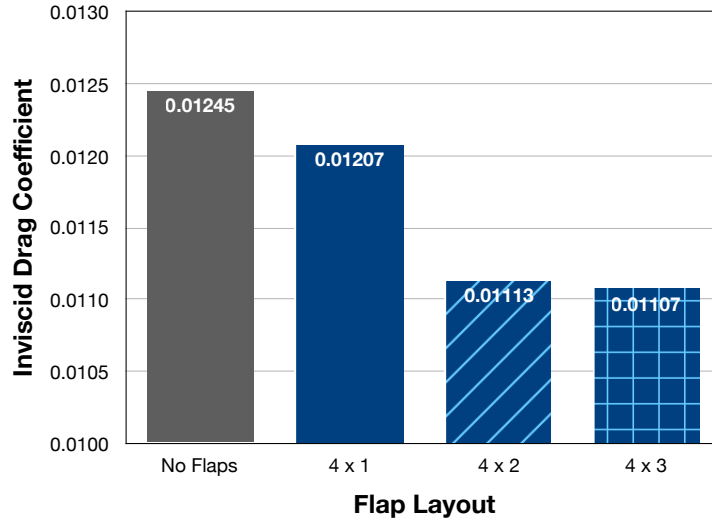


Figure 14. Distributed flap systems studied with 4 spanwise flaps. Different shades of blue represent individual flap chordwise segments while gold represents the elastomer between spanwise flaps.

Flap Layout	Total Lift Coefficient	Tail Lift Coefficient	Inviscid Drag Coefficient	Pitching Moment Coefficient	Wing Tip Deformation (inches)
None	0.4665	-0.0409	0.01245	-0.0008	149.5
4 x 1	0.4666	-0.0386	0.01207	0.0000	142.8
4 x 2	0.4664	-0.0426	0.01113	-0.0005	140.7
4 x 3	0.4667	-0.0437	0.01107	0.0004	141.3

Table I. Overspeed performance of optimized CRM configurations with 4 distributed flaps with varying number of segments as compared to CRM with no flaps.



**Figure 15. Overspeed drag of optimized configurations with 4 spanwise flaps with varying number of segments as compared to CRM with no flaps.**

The surface pressure contours on the wing with optimized flap settings are shown in Figure 16. The contours on the wing with no flaps are also shown for comparison. The contours clearly show a weakening of the main shock as flaps are deflected, particularly on the outboard part of the wing. Pressure distributions at the spanwise stations indicated in Figure 16 are shown in Figure 17. For both stations, the single segment flaps are able to slightly weaken the main wing shock which is likely the main source of drag reduction shown in Table I and Figure 15. The two-segment flaps are able to break this one strong shock into multiple weaker shocks, thus further reducing wave drag. Note that while inviscid analysis has been employed, the fact that shocks are weakened as a result of optimizing the flap deflections bodes well for confirmation via viscous analysis. Shock-induced separation should be delayed when the flaps are deflected accordingly.

Cross-sectional geometries of the flap region for all the wings in Figure 16 are shown in Figure 18. Note the similarity between the two- and three-segment flap deflected shapes, which explains the very similar performance. The single-segment deflected flap geometry lies in between the no-flap and multiple-segment-flap geometries. All of the deflected flap shapes effectively move the reflex of the airfoil toward the trailing edge. This is consistent with supercritical airfoil design trends as Mach number increases. Simply put, the flap systems allow the airfoil sections to morph towards shapes that perform better at higher Mach numbers, further verifying much of the improvement in performance is due to a reduction in wave drag.

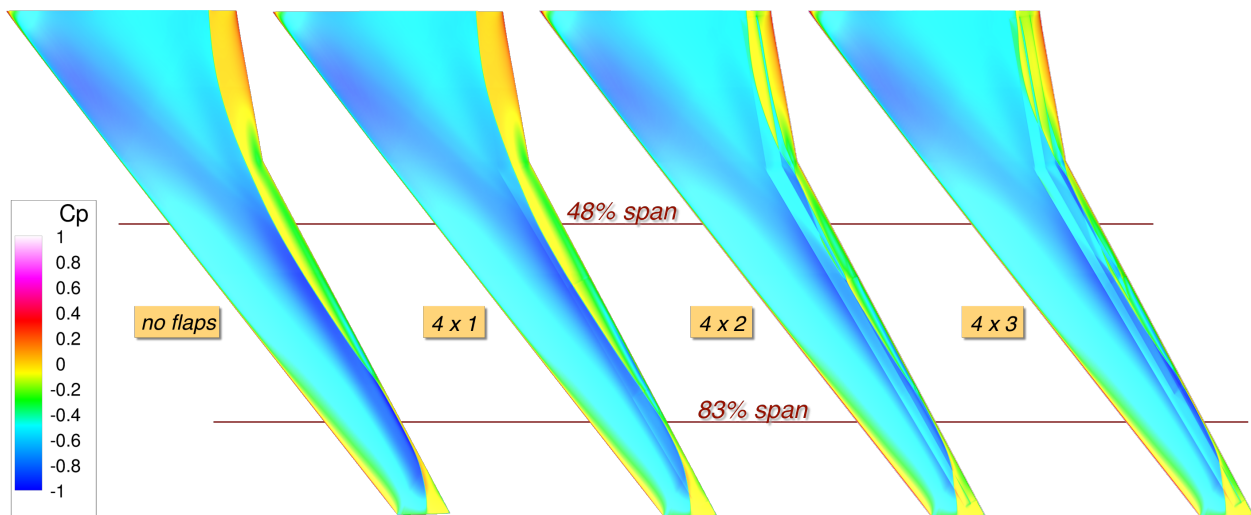


**Figure 16. Pressure contours on CRM wing without and with 4-flap layouts each optimized for the overspeed off-design condition.**

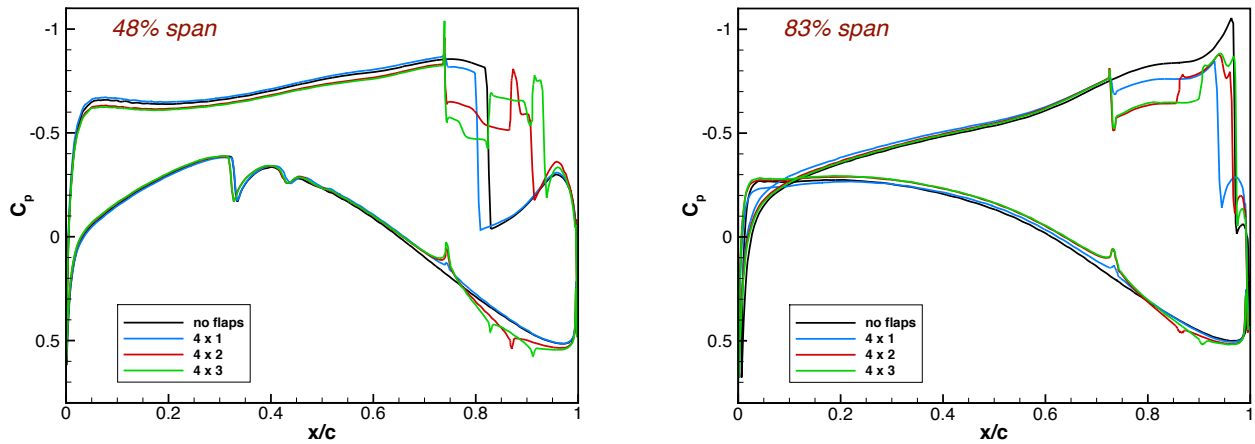


Figure 17. Pressure distributions on optimized CRM wings with 4-flap systems at two span stations.

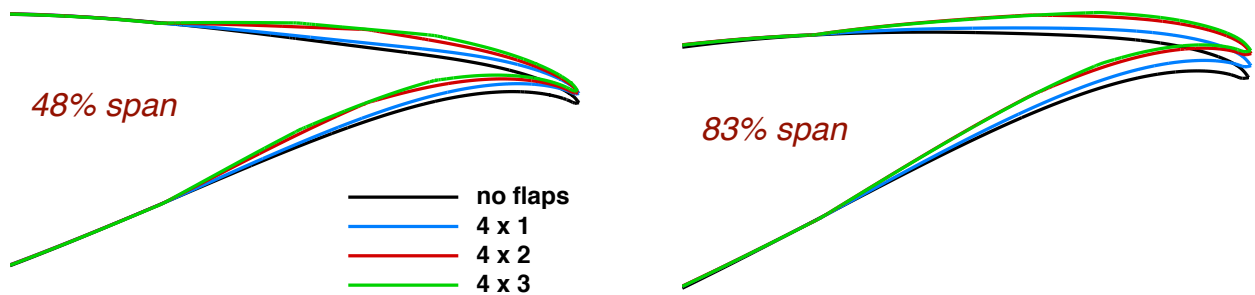


Figure 18. Optimized 4-flap geometry at two wing span stations as compared to the no-flap geometry. The vertical to horizontal scale is 4:1 for clarity.

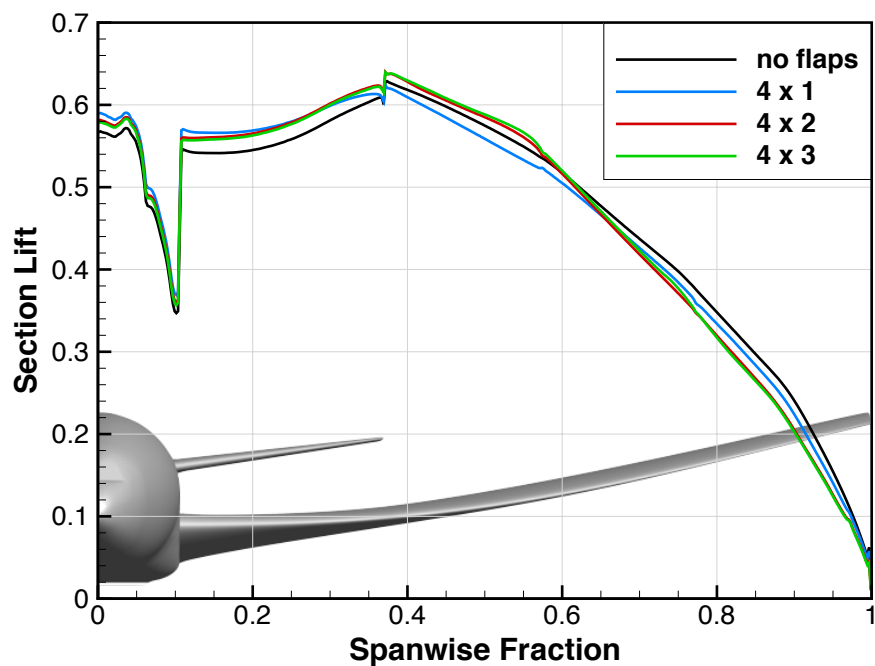


Figure 19. Spanwise lift distributions on CRM with optimized 4-flap systems.

In this inviscid analysis, the other source of drag computed is induced drag, which is a function of the spanwise lift distribution. The lift distribution on each of the wings is shown in Figure 19. Since the optimal lift distribution was not computed for the higher Mach number, the effects of the flap deflections on induced drag is not quantitative. However, the similarity of lift distributions suggests minimal effect on induced drag when the total drag improvements listed in Table I are considered. Also, note that pushing the trailing edge camber reflex backward increases the nose-down pitching moment of the wing, forcing the horizontal tail to contribute more down force and thus increasing induced drag. Clearly the optimized geometry has compromised on induced drag to reduce wave drag by a greater amount.

The next step in the trade study was to increase the number of spanwise flaps. While on a real airplane this would add weight for additional actuators and elastomer material, the performance benefits could be great enough to overcome these disadvantages. Two 8-flap systems were created and optimized. These two systems have one (8 x 1) and two (8 x 2) segments. A 3-segment system was not analyzed based on the results of the 4-flap systems. A 12-flap system was also optimized. Based on the results of the 4-flap systems, only the 2-segment version (12 x 2) was built. These three flap systems are depicted in Figure 20. The performance of these flap systems once optimized are given in Table II along with some previous results for comparison. The drag of all of the optimized flap systems are presented in the bar chart of Figure 21. These results are not nearly as dramatic as what was seen by adding flap segments to the 4-flap systems. The 12-flap system was able to improve performance by a bit less than 2 counts when compared to the 4-flap system with the same number of segments. In reality, the added complexity and weight of tripling the number of flaps would likely overwhelm this small improvement gain. What this suggests is that induced drag cannot be significantly improved in the the overspeed condition by adding more spanwise flaps. This is the second major takeaway from the trade study. The result also suggests that perhaps fewer than 4 spanwise flaps may be a viable option, at least for this off-design condition, particularly if the outboard flap spans are not identical as what was done in this trade study.

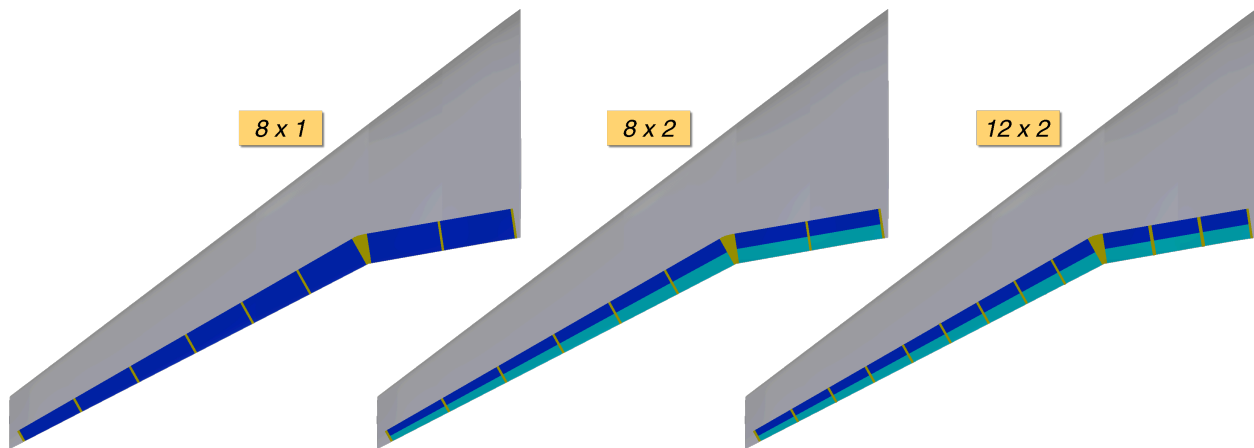
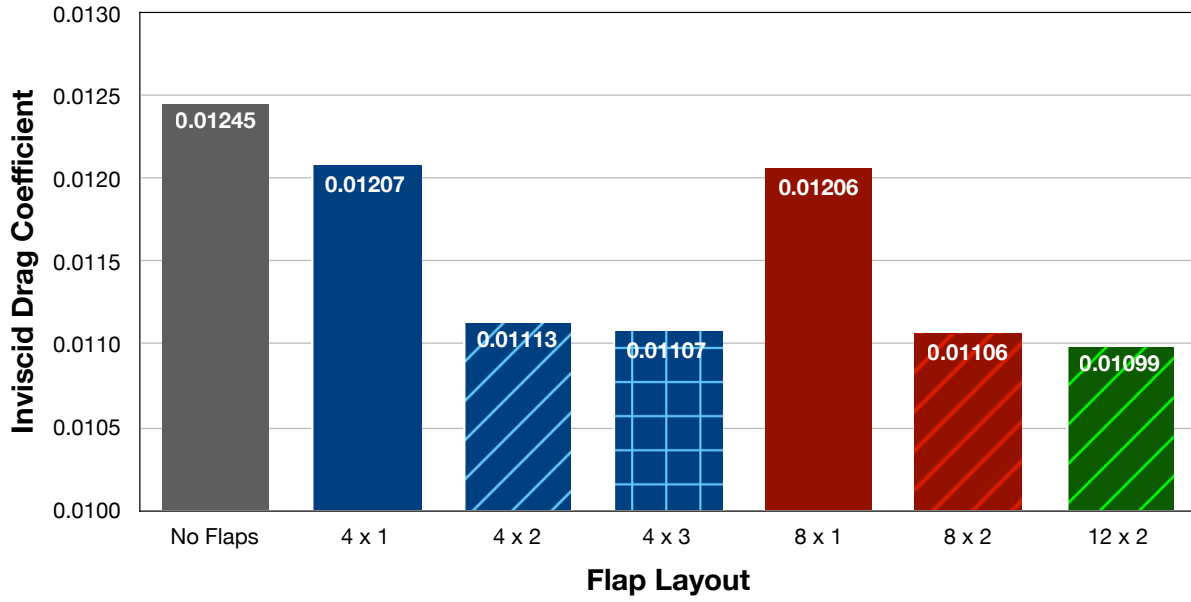


Figure 20. Distributed flap systems studied with 8 or 12 spanwise flaps. Different shades of blue represent individual flap chordwise segments while gold represents the elastomer between spanwise flaps.

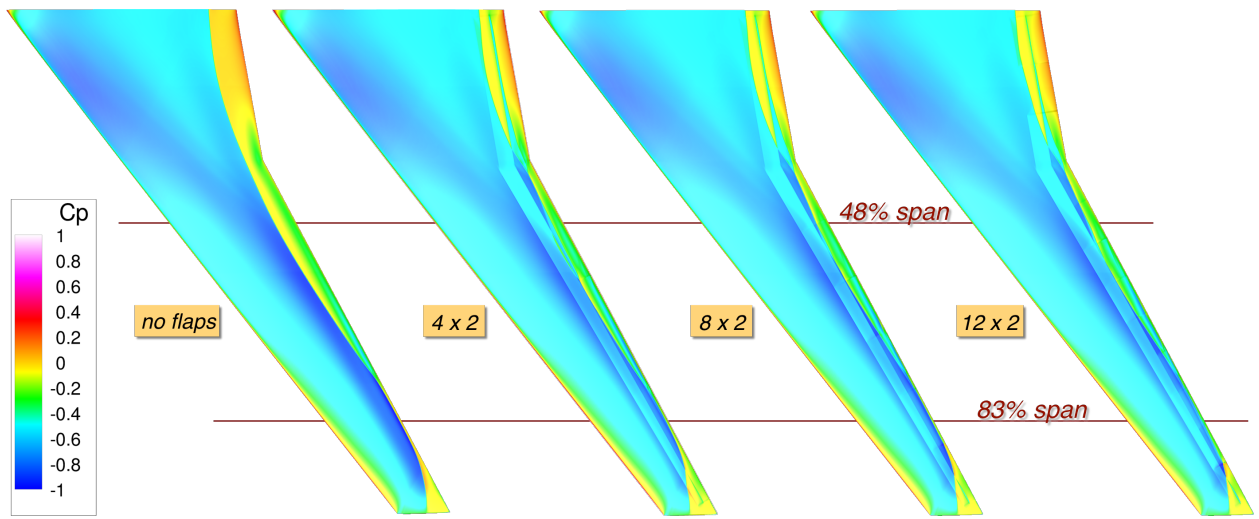
Flap Layout	Total Lift Coefficient	Tail Lift Coefficient	Inviscid Drag Coefficient	Pitching Moment Coefficient	Wing Tip Deformation (inches)
None	0.4665	-0.0409	0.01245	-0.0008	149.5
4 x 1	0.4666	-0.0386	0.01207	0.0000	142.8
8 x 1	0.4665	-0.0388	0.01206	0.0000	143.5
4 x 2	0.4664	-0.0426	0.01113	-0.0005	140.7
8 x 2	0.4665	-0.0432	0.01106	-0.0009	142.9
12 x 2	0.4665	-0.0431	0.01099	0.0003	142.7

Table II. Overspeed performance of optimized configurations with distributed flaps as compared to no flaps.



**Figure 21. Overspeed drag of optimized configurations with distributed flaps as compared to no flaps. Similar colors have the same number of spanwise flaps, while similar patterns have the same number of segments (except for the no flaps case).**

The pressure contours on the wings with optimized 2-segment flap deflections are shown in Figure 22, while pressure distributions at 48% and 83% semispan on these wings are given in Figure 23. Note the very similar contours and pressure distributions no matter how many spanwise flaps are used. This is consistent with the small difference in actual aerodynamic performance. The spanwise lift distributions for these optimized wings are presented in Figure 24. Once again, the differences here are small, presenting a consistent result that for this overspeed condition, relatively few spanwise flaps are necessary to achieve appreciable gains in aerodynamic performance.



**Figure 22. Pressure contours on CRM wing with no and 2-segment layouts each optimized for overspeed.**

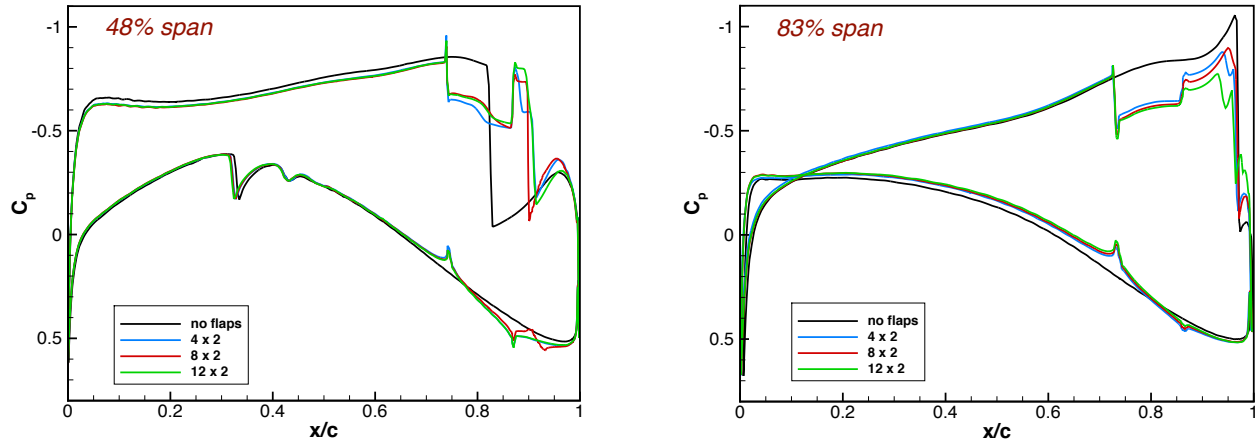


Figure 23. Pressure distributions on optimized CRM wings with 2-segment flap systems at two span stations.

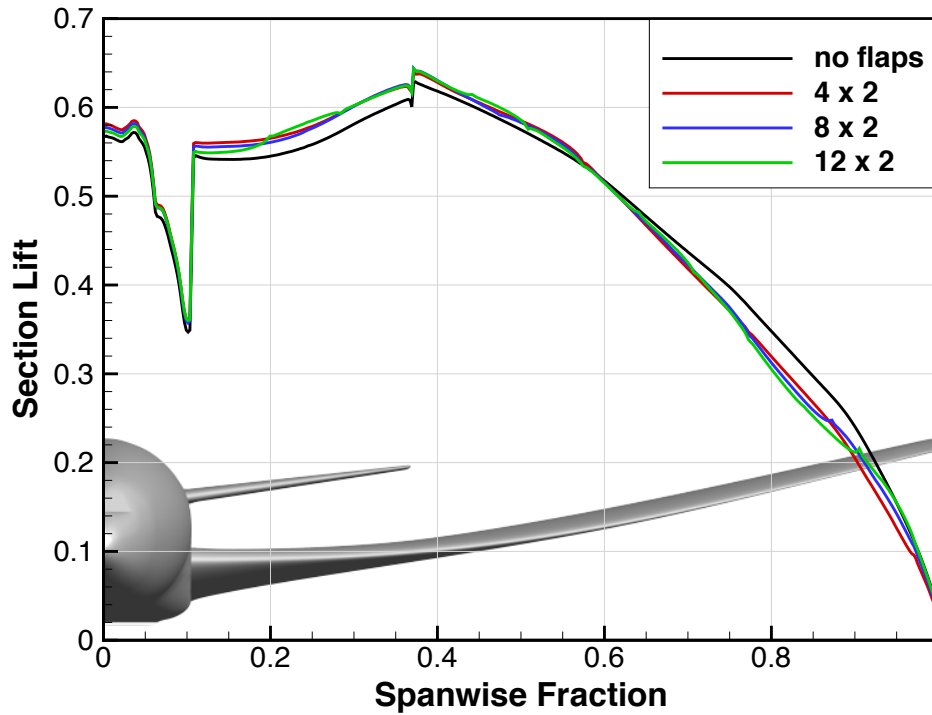


Figure 24. Spanwise lift distributions on CRM with optimized 2-segment flap systems.

For reference, the flap deflections on the optimized 4-flap, 2-segment wing are shown in Figure 25. The magnitude of the deflections (up to about  $2^\circ$ ) are typical for all of the optimized deflections of each layout considered in the trade study. The effective change in geometry is subtle but clearly effective at these high transonic Mach numbers.

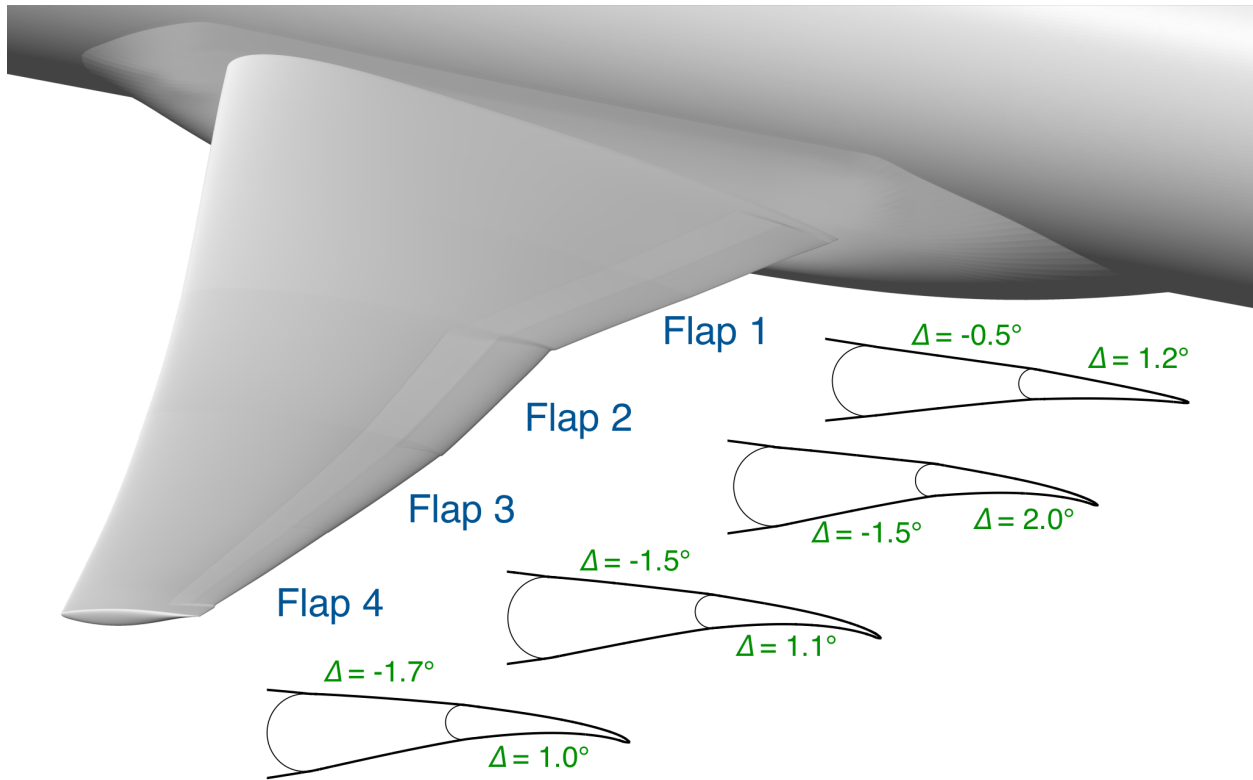


Figure 25. Deflections on 4 x 2 flap system optimized for overspeed. Positive angles are downward.

#### IV. Future Work

The results from the trade study presented in this work were rather conclusive for the overspeed flight condition. But these results were generated using an inviscid aerodynamic analysis. Re-computing the performance gains with a viscous analysis (such a RANS solver) could verify the results of the trade study. While Euler analysis at the cruise condition where very little separated flow is expected is often sufficient, double-checking these results with a viscous analysis would be worthwhile.

Of course, flying 3% faster than the cruise design point is not the only off-design condition a commercial transport may encounter or for which it must be designed. There are other off-design conditions that can be addressed by distributed flaps and doing so could have a major impact on the design of the aircraft. For instance, most aircraft must be designed for a maneuver case, where the aircraft must produce lift equal to say one and a half times its full weight. Such a flight condition is often the limiting case for the structural design. As has been shown before in many works such as that by Lebofsky,<sup>24</sup> distributed flaps can be used to offload the outboard portion of the wing thus reducing the wing root bending moment. If the maneuver case is indeed the limiting design point for the wing, the structure of a wing with distributed flaps could be significantly lighter which would have tremendous impact on the aircraft design overall. While the wing area is often set by the takeoff flight condition ( $C_{L,max}$ ), the aspect ratio is often limited by structural weight considerations. Lowering the wing weight could allow for a higher aspect ratio and thus improved cruise performance.

Using distributed flaps to reduce the wing structural weight clearly has an effect on several systems of the entire aircraft. Performing a trade study with a fixed structural model as was done for the overspeed case would not be sufficient. The structural design would have to be varied as well which means a complete aerostructural design capability would need to be applied. Also, inviscid analysis may not be sufficient either. Increased loading on the wing may induce flow separation, which obviously cannot be accurately predicted with an Euler solver. Hence, any future distributed flap study on the maneuver condition would benefit from viscous aerodynamic analysis. A viscous flow solver would also be useful at other flight conditions such as takeoff and landing. These are just some of the problems that could be tackled to further identify the potential benefits and drawbacks of distributed flap systems.

## V. Conclusions

A flap layout trade study was conducted on a highly-flexible CRM configuration that consisted of the fuselage, wing, and horizontal tail. The trade study goal was to determine the complexity of a full-span, distributed flap system that is necessary to provide meaningful aerodynamic performance benefits at an overspeed cruise flight condition. The number of spanwise flaps considered was 4, 8, or 12, where each flap consisted of up to three chordwise segments. The deflection of each flap segment was optimized for minimum drag while maintaining cruise lift and longitudinal trim. Comparing the results from each optimization with the same number of spanwise flaps showed that while one-segment flaps provide some performance benefit (roughly 4 counts), two-segment flaps were found to be particularly effective at reducing wave drag (a total of about 13 counts). Adding a third segment, however, did not provide significant benefit over the two-segment flap, no matter how many spanwise flaps were implemented. Comparing the results from the flap systems with the same number of segments but different number of spanwise flaps revealed different results. The 12-flap system did not produce significant benefit (less than 2 counts of drag) over even the 4-flap system, suggesting that systems that are simpler in the spanwise direction may be sufficient for the overspeed off-design condition. These results also suggest that for the overspeed condition, induced drag is either already near the optimum or cannot be significantly improved with these flap systems. In other words, wave drag seems to be the major driver in terms of determining the necessary complexity of a distributed flap system for the overspeed condition. This conclusion is supported by the fact that the downward force on the horizontal tail actually increased as overall drag decreased with every flap system studied. The overall conclusion of this work is that a distributed 4-flap, two-segment system is the simplest installation studied that can provide significant performance benefit for a highly flexible version of the CRM cruising at an overspeed condition.

## Acknowledgements

This work was partially supported by the Advanced Air Transport Technology Project of NASA's Aeronautics Research Mission Directorate. The authors acknowledge the guidance and supervision of Dr. Nhan Nguyen of NASA's Intelligent Systems Division at NASA Ames Research Center. David Rodriguez and George Anderson were supported by NASA Ames Research Center Contract NNA10DF26C. Computer support was provided by the NASA Advanced Supercomputing Center at NASA Ames. Nathan Precup of the University of Washington provided the undeformed version of the CRM wing.

## References

- <sup>1</sup>Nguyen, N. T., "NASA Innovation Fund Award 2010 Project: Elastically Shaped Future Air Vehicle Concept," NASA Rept. ARC-E-DAA-TN3743, 2010.
- <sup>2</sup>Nguyen, Nhan T., Trihn, K., Reynolds, Kevin, Kless, J., Aftosmis, M. J., "Elastically Shaped Wing Optimization and Aircraft Concept for Improved Cruise Efficiency," AIAA Paper 2013-0141, Jan. 2013.
- <sup>3</sup>Urnes, J., Nguyen, N, Ippolito, C., Totah, J., Trihn, K., and Ting, E., "A Mission-Adaptive Variable Camber Flap Control System to Optimize High Lift and Cruise Lift-to-Drag Ratios of Future N+3 Transport Aircraft," AIAA Paper 2013-0214, Jan. 2013.
- <sup>4</sup>Rodriguez, D. L., Aftosmis, M. J., Nemecek, M., and Anderson, G. R., "Optimization of Flexible Wings With Distributed Flaps At Off-Design Conditions," *Journal of Aircraft*, Vol. 53, No. 6 (Oct. 2016), pp. 1731-1745. doi:10.2514/1.C033535
- <sup>5</sup>Spillman, J. J., "The Use of Variable Camber to Reduce Drag, Weight and Costs of Transport Aircraft," *The Aeronautical Journal*, Vol. 96, No. 951 (1992), pp. 1-9.
- <sup>6</sup>Szodruch, J., and Hilbig, R., "Variable Wing Camber for Transport Aircraft," *Progress in Aerospace Sciences*, Vol. 25, No. 3 (1988), pp. 297-328. doi:10.1016/0376-0421(88)90003-6
- <sup>7</sup>Wakayama, S. R., and White, E. V., "Evaluation of Adaptive Compliant Trailing Edge Technology," AIAA Paper 2015-3289, June 2015.
- <sup>8</sup>Kota, S., Hetrick, J., Osborn, R., Paul, D., Pendleton, E., Flick, P., and Tilmann, C., "Design and Application of Compliant Mechanisms for Morphing Aircraft Structures," *Proceedings of SPIE Smart Structures and Materials*, Vol. 5054, Soc. of Photo-Optical Instrumentation Engineers, Bellingham, WA, Aug. 2003, pp. 24-33.
- <sup>9</sup>Burdette, D. A., Kenway, G. K., and Martins, J. R. R., "Aerostructural Design Optimization of a Continuous Morphing Trailing Edge Aircraft for Improved Mission Performance," AIAA Paper 2016-3209, June 2016.
- <sup>10</sup>Vassberg, J., Dehaan, M., Rivers, M., and Wahls, R., "Development of a Common Research Model for Applied CFD Validation Studies," AIAA Paper 2008-6919, Aug. 2008. doi:10.2514/6.2008-6919
- <sup>11</sup>Jordan, T., Langford, W., Belcastro, C., Foster, J., Shah, G., Howland, G., and Kidd, R., "Development of a Dynamically Scaled Generic Transport Model Testbed for Flight Research Experiments," *AUVSI's Unmanned Systems North America Symposium and Exhibition*, Anaheim, CA, 2004.
- <sup>12</sup>Rodriguez, D. L., Aftosmis, M. J., Nemecek, M., and Smith, S. C., "Static Aeroelastic Analysis With an Inviscid Cartesian Method," AIAA Paper 2014-0836, Jan. 2014. doi:10.2514/6.2014-0836

- <sup>13</sup>Nemec, M. and Aftosmis, M., “Parallel Adjoint Framework for Aerodynamic Shape Optimization of Component-Based Geometry,” AIAA Paper 2011-1249, Jan. 2011. doi:10.2514/6.2011-1249
- <sup>14</sup>Aftosmis, M. J., Berger, M. J., and Adomavicius, G., “A Parallel Multilevel Method for Adaptively Refined Cartesian Grids With Embedded Boundaries,” AIAA Paper 2000-0808, Jan. 2000. doi:10.2514/6.2000-808
- <sup>15</sup>Gallman, J. W. and Kroo, I. M., “Structural Optimization for Joined-Wing Synthesis,” *Journal of Aircraft*, Vol. 33, No. 1 (January-February 1996), pp. 214-223. doi:10.2514/3.46924
- <sup>16</sup>Aftosmis, M., Nemec, M., and Cliff, S., “Adjoint-Based Low-Boom Design With Cart3D,” AIAA Paper 2011-3500, June 2011. doi:10.2514/6.2011-3500
- <sup>17</sup>Wintzer, M., Kroo, I. M., Aftosmis, M. J., and Nemec, M., “Conceptual Design of Low Sonic Boom Aircraft Using Adjoint-Based CFD,” *Seventh International Conference on Computational Fluid Dynamics (ICCFD7)*, Big Island, HA, 2012.
- <sup>18</sup>Smith, S., Nemec, M., and Krist, S., “Integrated Nacelle-Wing Shape Optimization for an Ultra-High Bypass Fanjet Installation on a Single-Aisle Transport Configuration,” AIAA Paper 2013-0543, Jan. 2013. doi:10.2514/6.2013-543
- <sup>19</sup>Anderson, G., Aftosmis, M., and Nemec, M., “Parametric Deformation of Discrete Geometry for Aerodynamic Shape Design,” AIAA Paper 2012-0965, Jan. 2012. doi:10.2514/6.2012-965
- <sup>20</sup>Jordan, T. L., Langford, W. M., Belcastro, C. M., Foster, J. M., Shah, G. H., Howland, G., and Kidd, R., “Development of a Dynamically Scaled Generic Transport Model Testbed for Flight Research Experiments,” *AUVSI’s Unmanned Systems North America Symposium and Exhibition*, Arlington, VA, 2004.
- <sup>21</sup>Vassberg, J. C., Tinoco, E. N., Mani, M., Rider, B., Zickuhr, T., Levy, D. W., Brodersen, O. P., Eisfeld, B., Crippa, S., and Wahls, R. A., “Summary of the Fourth AIAA Computational Fluid Dynamics Drag Prediction Workshop,” *Journal of Aircraft*, Vol. 51, No. 4 (2014), pp. 1070-1089.
- <sup>22</sup>Chen, S., Lyu, Z., Kenway, G. K. W., and Martins, J. R. R. A., “Aerodynamic Shape Optimization of Common Research Model Wing–Body–tail Configuration,” *Journal of Aircraft*, Vol. 53, No. 1 (Sept. 2015), pp. 276-293. doi:10.2514/1.C033328
- <sup>23</sup>Kroo, I., “Tail Sizing for Fuel Efficient Transports,” AIAA Paper 1983-2476, Oct. 1983. doi:10.2514/6.1983-2476
- <sup>24</sup>Lebofsky, S., Ting, E., and Nguyen, N., “Multidisciplinary Drag Optimization of Reduced Stiffness Flexible Wing Aircraft With Variable Camber Continuous Trailing Edge Flap,” AIAA Paper 2015-1408, Jan. 2015.